Liquid Crystals
Publication details, including instructions for authors and subscription information:
http://www.informaworld.com/smpp/title~content=t713926090

Mesophases of hockey stick mesogens

F. C. Yu[a]; L. J. Yu[a]
[a] Department of Chemistry, Tamkang University, Tamsui, Taipei 25137, Taiwan

To cite this Article Yu, F. C. and Yu, L. J.(2008) 'Mesophases of hockey stick mesogens', Liquid Crystals, 35: 7, 799 — 813
To link to this Article: DOI: 10.1080/02678290802195697
URL: http://dx.doi.org/10.1080/02678290802195697

Liquid Crystals,
Vol. 35, No. 7, July 2008, 799–813

Taylor & Francis
Taylor & Francis Group

Mesophases of hockey stick mesogens

F. C. Yu and L. J. Yu*

Department of Chemistry, Tamkang University, Tamsui, Taipei 25137, Taiwan

(Received 22 March 2008; final form 12 May 2008)

Enantiotropic anticlinic smectic C (SmC_a), smectic C (SmC), smectic A (SmA) and nematic (N) phases of hockey stick molecules were obtained by tuning the length of hydrocarbon chain located at the *meta*-position to the carbon–carbon double bond of a stilbenyl moiety of calamitic mesogenic skeletons. The thermodynamic properties and some aspects of optical appearance of these phases are indiscernible from those of calamitic mesogens. Distinctions are noted such as the appearance of two-brush defects and two types of domains in the tilted smectic phases. X-ray results indicate the existence of clusters in the nematic phase and simple layer structure in the smectic phases. These phases exhibit electric field driven colour switching, and all the results imply that all three molecular axes are simultaneously aligned in the N and SmC phases, a behaviour unprecedented and different from those of conventional calamitic mesogens. Doping with a chiral calamitic mesogen results in formation of corresponding chiral N and ferroelectric SmC phases, but the effect for the SmC_a phase is not clear. Small and comparable values of spontaneous polarisation are obtained for the doped and non-doped phases. Molecular organisations of the SmC and SmCa phases are proposed and discussed.

Keywords: hockey stick molecule; synclinic phase; anticlinic phase; chiral dopant; ferroelectric phase; antiferroelectric phase

1. Introduction

Ferroelectric and antiferroelectric liquid crystals have been well documented since the first report by Meyer and co-workers on the calamitic chiral smectic C phase (*1, 2*). The confirmation of ferroelectric and antiferroelectric switching behaviours of B_2 phases formed by achiral bent (banana) molecules showed that the chiral unit is not required for such mesogens to exhibit these behaviours (*3*). Link *et al.* have shown that these switching behaviours are the resultant of the correlation of the bent conformation and the tilt of molecular director (*4*). More recently, thermotropic biaxial nematic phases were reported for the banana mesogens comprised of oxadiazole derivatives (*5*). These observations clearly indicated that the bent conformation plays an essential role for induction of these interesting properties.

Considering the shape of molecular geometry, a hockey stick molecule (a bent molecule with two arms greatly different in length) can be regarded as an intermediate between the calamitic (rod-like) and the banana (bent with roughly equal arms) molecules. It is interesting therefore to investigate the property of mesophase formed by this intermediate, the hockey stick molecule. Recently, several unusual behaviours have been observed in the mesophases formed by hockey stick molecules. An anticlinic structure is confirmed for a lower temperature smectic C phase on freestanding films of hockey stick molecules consisting of Schiff's base and cinnamate or benzoate by ellipsometry and depolarised optical microscopy studies (*6*). An iridescent texture was observed on an unidentified mesophase formed by a chiral as well as a racemic hockey stick molecule having the same multifluoro-substituted three-phenyl ring system (*7*). A helical chiral smectic A phase undergoing a first-order transition to a ferroelectric smectic C phase was observed for a hockey stick molecule of a four-phenyl ring system having an ester of chiral 2-octanol pointing to the lateral direction (*8*). Obviously, more examples would be helpful to reveal the phase structures and properties of phases formed by these relatively unexplored hockey stick molecules. The realisation of the relationship between the mesophase property and the molecular shape would be helpful for designing new mesogens.

It was reported previously that nematic (N), smectic C (SmC) and anticlinic smectic C (SmC_a) phases could be formed by hockey stick molecules with a 4-dodecyloxybenzoyloxy or a dodecyloxy unit in the lateral direction of the calamitic 3-ring or 4-ring skeleton shown in Scheme 1 (*9*). It was found that two-brush defects, i.e. indication of the anticlinic layer structure, appeared easily in the tilted smectic phases formed by the hockey stick molecules. These anticlinic smectic phase constitutes the intermediate phase between the conventional calamitic and banana mesophases. Texture and colour switching driven by

*Corresponding author. Email: ljyu@mail.tku.edu.tw

ISSN 0267-8292 print/ISSN 1366-5855 online

DOI: 10.1080/02678290802195697
http://www.informaworld.com

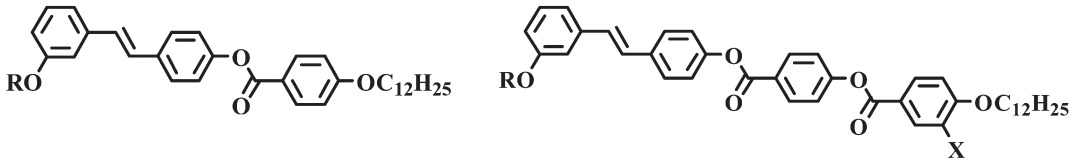

3-ring skeleton **4-ring skeleton**

Scheme 1. 3-ring and 4-ring calamitic skeletons.

electric fields was observed for these mesophases, but the corresponding spontaneous polarisations remained to be substantiated. The SmC_a phases were found to be monotropic (*9*). In this paper, it is shown that, in addition to the N and SmC phases, enantiotropic SmC_a phases with wide thermal range can be obtained by tuning the lateral chain length. These phases were converted to the corresponding chiral phases by addition of a chiral calamitic dopant. The electric properties for phases with and without the chiral dopant were studied and compared. A molecular organisation in the smectic phases of these hockey stick molecules is proposed on the basis of the observations presented.

2. Experimental

Scheme 2 shows the synthetic routes for obtaining the hockey stick molecules. A solution of 3-bromophenol, alkyl bromide, K_2CO_3 and dry acetone was refluxed to afford 3-alkoxy-bromobenzene (**I-n**). The Heck reaction (*10*) was carried out and followed by deprotection to obtain the hydroxyl stilbene derivatives (**II-n**). The phenol was esterified with different benzoic acid

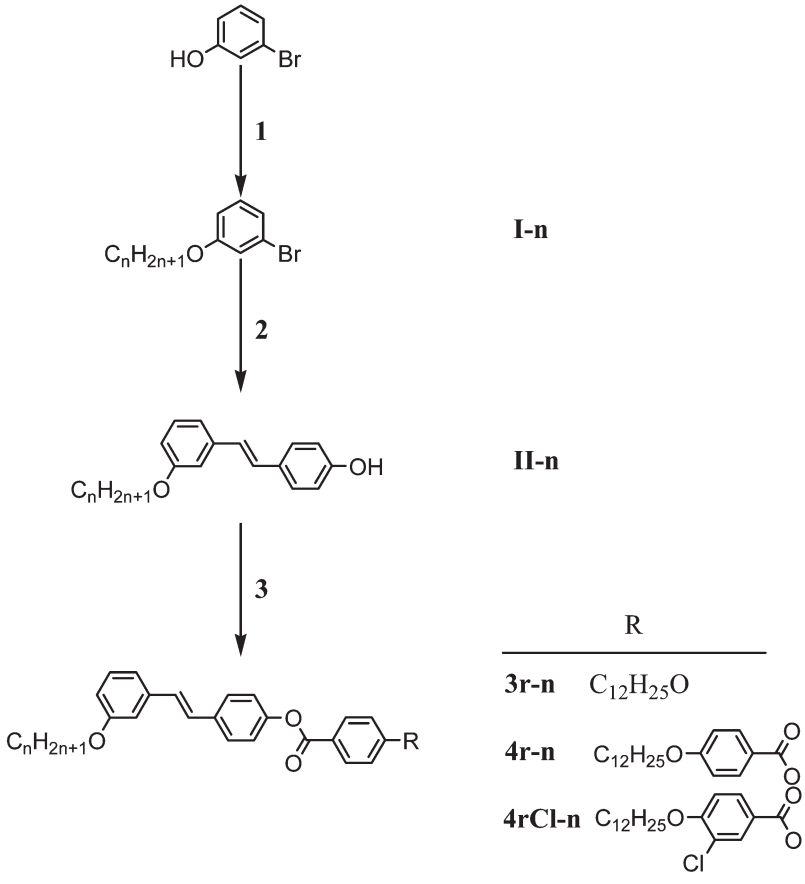

Scheme 2. Synthetic routes for hockey stick molecules consisting of a stilbenyl skeleton. (1) Alkyl bromide, K_2CO_3, acetone, 12 h. (2) (a) Acetoxystyrene, $Pd(OAc)_2$, (*o*-tol)$_3$P, CH_3CN, Et_3N, 36 h; (b) KOH, THF, CH_3OH, 2 h. (3) Dodecyloxybenzoic acid or 4-(4′-dodecyloxybenzoyloxy)benzoic acid or 4-(3′-chloro-4′-dodecyloxybenzoyloxy)benzoic acid, DCC, DMAP, THF, 24 h.

derivatives, with the aid of DCC/DMAP (*11*), to obtain the final products **3r-n, 4r-n** and **4rCl-n**.

Mesophase textures were studied by polarising optical microscopy (POM, Nikon Optiphot-POL) in conjunction with a temperature controller (Mettler FP 80HT and 82HT). The phase transitions were examined by differential scanning calorimetry (DSC, Perkin-Elmer Pyris 1). Electric-field effects were studied using dc and ac fields, and the method of triangular-wave voltage with different frequencies. X-ray diffraction for the non-aligned sample was conducted at the National Synchrotron Radiation Research Center (NSRRC, beam line 17A1), Taiwan.

Synthesis

*Synthesis of 3-alkoxybromobenzene (**I-n**)*

For 3-heptoxybromobenzene (**I-7**), 1-bromoheptane (8.95 g, 50 mmol) and 3-bromophenol (8.65 g, 50 mmol) were dissolved with anhydrous acetone (50 ml) and anhydrous potassium carbonate (6.91 g, 50 mmol) was added to the mixture, which was refluxed for 12 h. After work up, the residue was purified by vacuum distillation to give compound **I-7** (b.p. 88C/8 mmHg) with a yield of 80.8%. ^{1}H NMR ($CDCl_3$): δ 0.89 (t, J=6.9 Hz, 3H, C**H**$_3$), 1.29 (m, 8H, C**H**$_2$), 1.76 (m, 4H, C**H**$_2$CH$_2$O), 3.92 (t, J=6.6 Hz, 4H, C**H**$_2$O), 6.80 (dd, 1H, Ar–**H**), 7.04 (s, 1H, Ar–**H**), 7.05 (dd, 1H, Ar–**H**), 7.13 (t, J=8.4 Hz, 1H, Ar–**H**).

*Synthesis of 3-alkoxy-4′-hydroxystilbene (**II-n**)*

For 3-heptoxy-4′-hydroxy-stilbene (**II-7**), to a high-pressure bottle containing a mixture of compound **I-7** (8.13 g, 30 mmol), 4-acetoxystyrene (4.86 g, 30 mmol), palladium acetate (30 mg, 0.014 mmol),and tri-*o*-tolylphosphine (150 mg, 0.049 mmol) was added a mixed solvent triethylamine/acetonitrile (10/20 ml) before heating for 36 h under nitrogen. After work up, the crude product and potassium hydroxide (1.68 g, 30 mmol) were refluxed in THF-MeOH for 2 h followed by acidification. Compound **II-7** was obtained after recrystallisation from acetone/*n*-hexane with a yield of 51.2%, m.p. 93.5°C. ^{1}H NMR (300 MHz, $CDCl_3$): δ 0.90 (t, J=6.3 Hz, 3H, C**H**$_3$), 1.32 (m, 8H, C**H**$_2$), 1.80 (m, 4H, C**H**$_2$CH$_2$O), 3.99 (t, J=6.6 Hz, 4H, C**H**$_2$O), 4.72 (s, 1H, O**H**), 6.77 (dd, 1H, Ar–**H**), 6.81 (d, J=8.7 Hz, 2H, Ar–**H**), 6.95 (d, J=16.3 Hz, 1H, C**H**=CH), 7.01 (d, J=16.3 Hz, 1H, CH=C**H**), 7.02 (dd, 1H, Ar–**H**), 7.07 (s, 1H, Ar–**H**), 7.25 (t, J=8.0 Hz, 1H, Ar–**H**), 7.39 (d, J=8.6 Hz, 2H, Ar–**H**). IR (KBr, cm^{-1}) 968 (alkene *trans* C–H oop bend), 1045, 1240 (ether C–O stretch), 1512, 1592 (Ar C=C stretch), 2852, 2916 (alkane C–H stretch), 3252 (O–H stretch).

*Synthesis of 3-alkoxy-4′-(4″-dodecyloxybenzoyloxy)-stilbene (**3r-n**)*

For 3-heptoxy-4′-(4″-dodecyloxybenzoyloxy)stilbene (**3r-7**), to an Erlenmeyer flask containing a mixture of compound **II-7** (0.31 g, 1 mmol), 4-dodecyloxybenzoic acid (0.31 g, 1 mmo) and 4-(dimethylamino)pyridine (DMAP, 0.002 g, 0.1 mmol) was added 10 ml of anhydrous THF and 1,3-dicyclohexylcarbodiimide (DCC, 0.21 g, 1 mmol) and whole mixture was stirred at room temperature for 24 h. After work up, compound **3r-7** was recrystallised from THF-methanol with a yield of 46.8%. ^{1}H NMR (300 MHz, $CDCl_3$): δ 0.89 (m, 6H, C**H**$_3$), 1.28 (m, 26H, C**H**$_2$), 1.81 (m, 4H, C**H**$_2$CH$_2$O), 4.03 (m, 4H, C**H**$_2$O), 6.80 (dd, 1H, Ar–**H**), 6.96 (d, J=8.9 Hz, 2H, Ar–**H**), 7.05 (dd, 1H, Ar–**H**), 7.06 (d, J=16.4 Hz, 1H, C**H**=CH), 7.09 (d, J=16.4 Hz, 1H, CH=C**H**), 7.10 (s, 1H, Ar–**H**), 7.19 (d, J=8.6 Hz, 2H, Ar–**H**), 7.26 (t, J=8.8 Hz, 1H, Ar–**H**), 7.54 (d, J=8.6 Hz, 2H, Ar–**H**), 8.13 (d, J=8.9 Hz, 2H, Ar–**H**). IR (KBr, cm^{-1}) 968 (alkene *trans* C–H oop bend), 1166 (ether C–O stretch), 1263 (ester C–O stretch), 1506, 1608 (Ar C=C stretch), 1734 (ester C=O stretch), 2852, 2922 (alkane C–H stretch). Elemental analysis: for $C_{40}H_{54}O_4$ (%), found (calculated) C 80.27 (80.22), H 9.10 (9.09).

*Synthesis of 3-alkoxy-4′-(4″-(4‴-dodecyloxybenzoyloxy)benzoyloxy)stilbene (**4r-n**) and 3-alkoxy-4′-(4″-(3‴-chloro-4‴-dodecyloxybenzoyloxy)benzoyloxy)-stilbene (**4rCl-n**)*

Compounds of series **4r** and **4rCl** were synthesised similarly but with 4-(4′-dodecyloxybenzoyloxy)-benzoic acid for series **4r-n** and 4-(3′-chloro-4′-dodecyloxybenzoyloxy)benzoic acid for **4rCl-n**.

For 3-heptoxy-4′-(4″-(4‴-dodecyloxybenzoyloxy)-benzoyloxy)stilbene (**4r-7**), yield 41.7%. ^{1}H NMR (300 MHz, $CDCl_3$): δ 0.89 (m, 6H, C**H**$_3$), 1.28 (m, 26H, C**H**$_2$), 1.81 (m, 4H, C**H**$_2$CH$_2$O), 4.01 (t, J=6.6 Hz, 2H, C**H**$_2$O), 4.06 (t, J=6.5, 2H, C**H**$_2$O), 6.80 (dd, 1H, Ar–**H**), 6.97 (d, J=8.9 Hz, 2H, Ar–**H**), 7.05 (dd, 1H, Ar–**H**), 7.07 (d, J=16.3 Hz, 1H, C**H**=CH), 7.09 (d, J=16.3 Hz, 1H, CH=C**H**), 7.11 (s, 1H, Ar–**H**), 7.21 (d, J=8.5 Hz, 2H, Ar–**H**), 7.29 (t, J=8.9 Hz, 1H, Ar–**H**), 7.36 (d, J=8.8 Hz, 2H, Ar–**H**) 7.55 (d, J=8.7 Hz, 2H, Ar–**H**), 8.14 (d, J=8.8 Hz, 2H, Ar–**H**), 8.27 (d, J=8.7 Hz, 2H, Ar–**H**). IR (KBr, cm^{-1}): 962(alkene *trans* C–H oop bend), 1165 (ether C–O stretch), 1273 (ester C–O stretch), 1608, 1506 (Ar C=C stretch), 1734 (ester C=O stretch), 2922, 2852 (alkane C–H stretch). Elemental analysis: for $C_{47}H_{58}O_6$ (%),found (calculated) C (78.55 (78.52), H 8.15 (8.13).

For 3-heptoxy-4′-(4″-(3‴-chloro-4‴-dodecyloxy-benzoyloxy)- benzoyloxy)-stilbene (**4rCl-7**): yield

Table 1. Phase transition temperatures (°C) and the corresponding enthalpy changes (kJ mol^{-1}, in italics) of compounds **3r-n**.

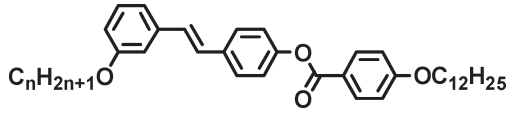

Compound	Cr			SmC$_a$		SmC		SmA		I
3r-4	·	74.4	·	81.8	·	83.1	·	86.7	·	
		29.76		*0.26*		*0.16*		*4.09*		
3r-6	·	77.1	·	81.8	·	83.4	·	84.0	·	
		53.06		*0.25*		*0.38*		*3.45*		
3r-7		73.1	(·)[b]	(71.8)[b]	·	83.5	·	83.9	·	
		54.19		*0.07*		[a]		*5.16*		
3r-8	·	70.6	·	79.6	·	84.4	·	84.7	·	
		47.84		*0.12*		[a]		*4.61*		
3r-10	·	81.2	(·)[b]	(69.0)[b]	(·)[b]	(81.2)[b]	–		·	
		59.52		*0.03*		*5.19*				
3r-12	·	77.2	–		·	80.1	·	80.3	·	
		66.95				*0.03*		*4.11*		

[a]Overlapped with the isotropisation transition. [b]Parentheses indicate monotropic.

47.0%. ^{1}H NMR (300 MHz, $CDCl_3$): δ 0.89 (m, 6H, C**H**$_3$), 1.28 (m, 26H, C**H**$_2$), 1.81 (m, 2H, C**H**$_2$CH$_2$O), 1.90 (m, 2H, C**H**$_2$CH$_2$O), 4.01 (t, J=6.5 Hz, 2H, C**H**$_2$O), 4.14 (t, J=6.6 Hz, 2H, C**H**$_2$O), 6.81 (dd, 1H, Ar–**H**), 6.99(d, J=8.7 Hz, 1H, Ar–**H**), 7.06 (dd, 1H, Ar–**H**), 7.07 (d, J=16.4 Hz, 1H, C**H**=CH), 7.09 (d, J=16.4 Hz, 1H, CH=C**H**), 7.11 (s, 1H, Ar–**H**), 7.21 (d, J=8.6 Hz, 2H, Ar–**H**), 7.27 (t, J=7.9 Hz, 1H, Ar–**H**), 7.36 (d, J=8.7 Hz, 2H, Ar–**H**), 7.56 (d, J=8.7 Hz, 2H, Ar–**H**), 8.07 (dd, 1H, Ar–**H**), 8.23 (d, J=2.1 Hz, 1H, Ar–**H**), 8.28 (d, J=8.7 Hz, 2H, Ar–**H**). IR (KBr, cm^{-1}): 974 (alkene *trans* C–H oop bend), 1166 (ether C–O stretch), 1273 (ester C–O stretch), 1506, 1597 (Ar C=C stretch), 1728 (ester C=O stretch), 2922, 2852 (alkane C–H stretch). Elemental analysis: for $C_{47}H_{57}ClO_6$ (%), found (calculated) C 74.92 (74.93), H 7.63 (7.63).

3. Results and discussion

Anticlinic smectic phase stabilised by tuning the meta-chain length

The mesophases and the corresponding thermal data for derivatives **3r-n** consisting of a three-ring skeleton are listed in Table 1. The length of hydrocarbon chain at the *meta*-position is increased from 4 to 12 carbon atoms to enhance the bent conformation, and a dodecyloxy chain is used at the *para*-position to ensure formation of smectic phases. A corresponding phase diagram is shown in Figure 1. It can be seen clearly that derivatives with longer chains have lower isotropisation temperatures, the exceptions being heptoxy- and octoxy-compounds. The crystal to mesophase temperature shows an irregular variation. Compound **3r-10** melts directly into isotropic so the SmC and SmCa phases are monotropic. The SmC$_a$ phase of **3r-7** is also monotropic. The thermal range of the SmA phase narrows with increasing chain length; SmA disappears for **3r-10** and reappears for **3r-12**. It is not clear whether the reappeared SmA phase is identical to that of the shorter chain derivatives. The main observation here is that the stabilisation of the tilted smectic phases can be achieved by shortening the chain length attached at the *meta*-position. The textures observed are the same as those reported previously (*9*), i.e. two- and four-brush defects for the SmC phase and mainly two-brush defects for the SmC$_a$ phase. For derivative **3r-12** the chain is too long such that the bent conformation renders the mesophasic packing of molecules unfavourable. The

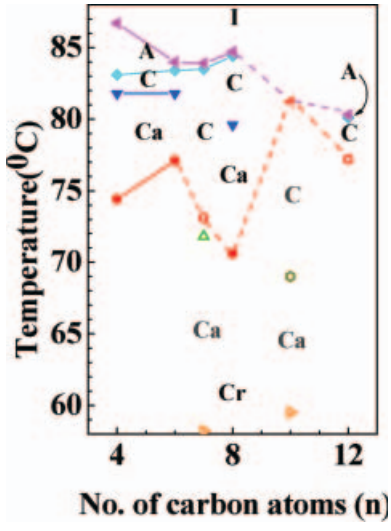

Figure 1. Phase diagram of the hockey stick homologues **3r-n**. The abbreviation Sm for smectic is omitted from the labelling for clarity.

Table 2. Phase transition temperatures (°C) and the corresponding enthalpy changes (kJ mol^{-1}, in italics) of compounds **4r-n** and **4rCl-n**.

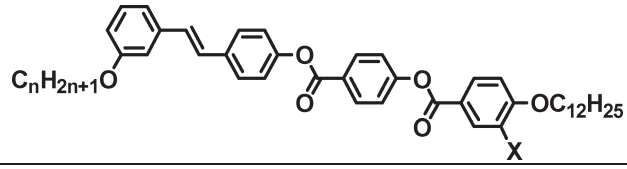

Compound	Cr		SmC_a		SmC		SmA		N		I
4r-4	·	108.0	·	133.2	·	166.4	·	169.6	·	186.2	·
		42.54		*0.18*		*0.53*		*0.52*		*0.64*	
4r-6	·	93.2	·	131.0	·	166.5	–		·	179.0	·
		33.98		*0.12*		*1.13*				*0.71*	
4rCl-6	·	109.5	–		·	154.8	–		·	159.3	·
		26.66				*3.18*				*0.67*	
4r-7	·	92.6	·	120.8	·	166.2	–		·	176.7	·
		34.83		*0.08*		*1.36*				*0.73*	
4rCl-7	·	108.5	–		·	154.8	–		·	157.5	·
		26.6				*3.71*				*0.80*	
4r-8	·	91.7	·	123.6	·	166.0	–		·	174.6	
		33.54		*0.06*		*1.53*				*0.82*	
4r-10	·	90.17	·	110.0	·	163.7	–		·	169.6	·
		39.82		*0.04*		*1.42*				*1.01*	
4r-12	·	91.8	(·)[a]	(86.6)[a]	·	161.4	–		·	165.7	·
		52.01		*0.02*		*1.30*				*1.26*	

[a]Parentheses indicate monotropic transition.

thermal range of mesophases of shorter chain members is about 10 K. Compared to the conventional calamitic three-ring mesogens, this drastically shortened mesophase range is apparently due to the bent conformation.

Listed in Table 2 are the mesophases and the corresponding enthalpy changes for homologues **4r-n** with four phenyl rings as the main skeleton with a dodecyloxy chain at the *para*-position and various chain lengths at the *meta*-position. The corresponding phase diagram is shown in Figure 2. It can be seen clearly from this figure that upon increasing the chain length at the *meta*-position the isotropisation temperature keeps decreasing, whereas the SmC–N transition temperature is nearly constant. The SmC–SmC_a transition temperature also decreases with increasing *meta*-position chain length, whereas the crystal–SmC_a remains nearly the same. The shortest member, **4r-4**, is exceptional; a short thermal range of SmA and a slightly higher Cr–SmC_a temperature are observed. A dip on the SmC–SmC_a transition temperature is observed for the heptoxy-member probably due to the odd number of carbon atoms of the hydrocarbon chain, a behaviour frequently encountered in the calamitic mesogens. Compared to the **3r-n** homologues, the thermal range and the corresponding temperatures are higher, as expected. The occurrence of N phases in the **4r-n** derivatives is interesting and apparently is due to the extra benzoate unit, which would bring in extra polarisability and hence strengthen the intermolecular force. The narrowing of the thermal range of this N phase with increasing *meta*-position chain length is understandable. It is due to the lowering of the isotropisation temperature and the occurrence of the smectic phase; both are frequently observed for the calamitic mesogens. The peculiar thing is that the occurrence of the SmC phase starts from the members of shorter chains as compared to the calamitic homologues. The thermal range of tilted smectic phases (SmC and SmC_a) is over 70 K, and about half or one third of

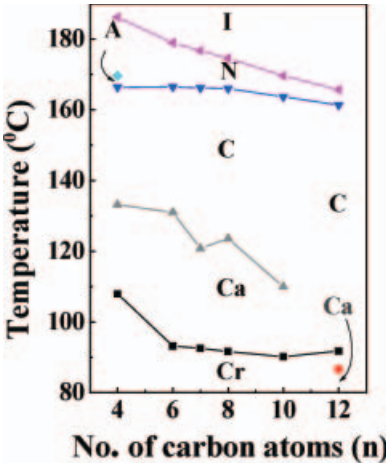

Figure 2. Phase diagram of the hockey stick homologues **4r-n**. The abbreviation Sm for smectic is omitted from the labelling for clarity.

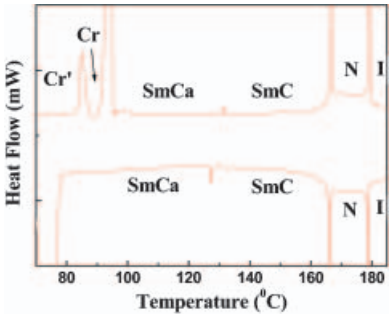

Figure 3. DSC thermograms of compound **4r-6**, displaying sharp peaks for the SmC–SmC$_a$ transition on heating and cooling scans, upper and lower, respectively.

which is of SmC$_a$. Apparently the bent conformation induces preferentially the tilted smectic phase, particularly the anticlinic layer structure. The preferred chain length for the SmC$_a$ to occur is six or eight carbon atoms, similar to that observed for **3r-n** series. The monotropic SmC$_a$ phase of compound **4r-12** is ascribed to the long chain effect. Also listed in Table 2 are the results of derivatives with a chlorophenyl replacing the terminal phenyl ring; **4rCl-6** and **4rCl-7**. The isotropisation temperatures were lowered by 20 K and the crystal to mesophase temperatures were elevated by 16 K as compared to those of analogous derivatives without a chlorine atom. The consequence is a narrowing of thermal range for both N and SmC phases, and the SmC$_a$ phase is not detected. Apparently the sophisticated molecular organisation is severely affected by the size and dipole moment inherited from the chlorine atom. Similar pronounced effects have been observed for several banana mesogens (*12*).

The values of enthalpy change for the SmA–I transition of homologues **3r-n**, listed in Table 1, are of the same order of magnitude as the typical values of calamitic mesogens. For homologues **4r-n**, listed in Table 2, the enthalpy changes for the N–I transition is less than 1 kJ mol^{-1}, except for the last two members studied here. This value is about one order of magnitude smaller than that of SmA–I transitions of **3r-n**, and is comparable to that observed for calamitic mesogens. For the smectic–nematic transition for **4r-n**, the enthalpy change is comparable to that of calamitic mesogens. For the SmC–SmC$_a$ transitions of both series a peak is evident in the DSC scans although with a very small value of enthalpy change. A typical thermogram is shown in Figure 3 for compound **4r-6** as an example. These very small values of enthalpy change indicate that the transition is weakly first order, a behaviour differing slightly from that of calamitic mesogens. Aside from this aspect, all other thermodynamic data indicate that the thermal behaviours of mesophases formed by these hockey stick molecules are not discernable from those of calamitic mesophases.

The electric field driven activities

The nematic phase of compounds **4r-n** can be aligned with substrate surfaces coated with polyimide and buffed to give very uniform homogeneous textures with rather strong optical fluctuation. In this state they are not distinguishable from the nematic phases of typical calamitic mesogens. The electric-field driven activities are, however, entirely different. Figure 4 shows the effect of an electric field on the nematic phase of **4r-8** in an EHC cell of 5 µm thickness with surfaces treated for parallel alignment. Uniform colour textures are observed when the aligning direction is rotated 45° with respect to the crossed polarisers (Figure 4(a)). Upon application of an ac electric field, the textures remain static but exhibit uniform colour changes with increasing field strength (Figure 4(b)). At slightly higher fields, static textures of various degrees of grey colour and with a much less optical fluctuation are observed (Figures 4(c) and 4(d)). These behaviours have never been encountered before for the nematic phases of calamitic mesogens, and strongly indicate that all three axes of the molecules are aligned by the applied field (*5a–c*). For a 15 µm thick cell (similar surface treatments) filled with **4r-8**, stripe patterns (*9*), colour variations and turbulence were observed with increasing field strength. Evidently the sample thickness plays a certain role in the field driven activities for the nematic phases formed by these hockey stick molecules.

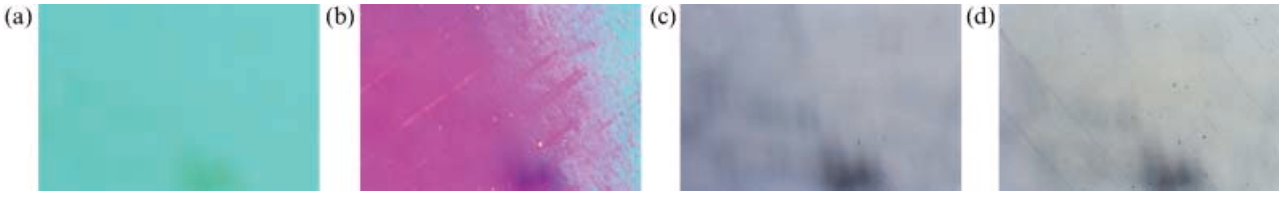

Figure 4. Electric field effect on the nematic textures of **4r-8** at 167.0°C, under crossed polarisers (polarization parallel to the edges of the photomicrograph). Homogeneous alignment, rubbing direction rotated 45°, 5 µm thickness. Applied ac electric field (60 Hz) was (a) 0, (b) 0.4, (c) 1 and (d) 4 V µm^{-1}. The horizontal edge is 0.375 mm.

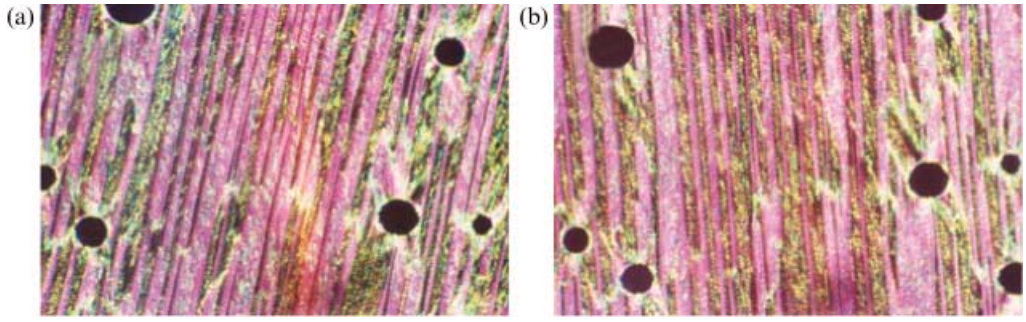

Figure 5. Textures of SmC phase of **4r-8** at 147.8°C in a cell of 5 μm thickness treated for parallel alignment. The neighbouring domains exchange their birefringence when the sample is rotated to opposite directions (a) 9° and (b) −7°. The horizontal edge is 0.75 mm.

On cooling the nematic phase of **4r-8** to the smectic phase in an EHC cell (parallel alignment, 5 μm thickness), the nematic texture developed into elongated domains of two different colours (birefringence) with equal fraction of area (Figure 5). There are equally spaced parallel lines across all the domains. The direction of these lines makes an angle with respect to the domain long axis, and point to the opposite direction for neighbouring domains. These domains will exchange colours when the sample is rotated to opposite direction. When this rotation angle is higher than 15°, the texture is brighter and the difference in birefringence diminishes slightly (Figure 6(b)). With application of a dc field, the domain textures do not change, but colour switching is obvious (Figure 6(a)) and the parallel lines within the domains are not observable. The colours of these domains remain the same with reversing field polarity (Figures 6(a) and 6(c)) but exchange between neighbouring domains if the rotation angle is reversed. These behaviours are similar to those reported previously (*9*).

The enantiotropic behaviour of the SmC_a phase for the compounds presented here provided a convenient condition to work on. Cooling the SmC phase of **4r-8** to the SmC_a phase, the elongated domains remain roughly the same and are of two different colours. Overlapped on the domains are rectangular grids (which look like a cartridge belt pattern), and some are square grids, as shown in Figure 7. This pattern results from growth of stripes originating from the domain boundary and propagating in a direction nearly perpendicular to the domain long axes. The grooves parallel to the domain long axis developed simultaneously and resulted in the grid-like pattern. The colours of neighbouring domains are exchanged when the sample is rotated in the opposite direction (Figure 7) similar to that observed for the SmC texture. When the alignment direction is rotated by an angle 45° with respect to the crossed polarisers, the colour is more uniform across the sample (Figure 8(a)). Upon application of dc fields, variation in colour starts to appear and becomes more pronounced with increasing field strength (Figures 8(b)–8(d)). The texture returns to the original texture of zero-field when the electric field is turned off. However, when the field polarity is inverted there is no discernable difference in the textures observed, similar to the behaviour observed for the SmC phase.

It should be noted that when a relatively high dc voltage (about 280–300 V) is applied to this SmC_a phase, the wriggled lines (the pitch band-like equidistance parallel lines) disappear and the texture is

Figure 6. Field effect on the SmC phase of **4r-8** at 155.0°C in a cell of 5 μm thickness treated for parallel alignment. The alignment direction is rotated by 15°. The applied sc field was (a) 2.6, (b) 0 and (c) $-2.6\,V\,\mu m^{-1}$. The horizontal edge is 0.75 mm.

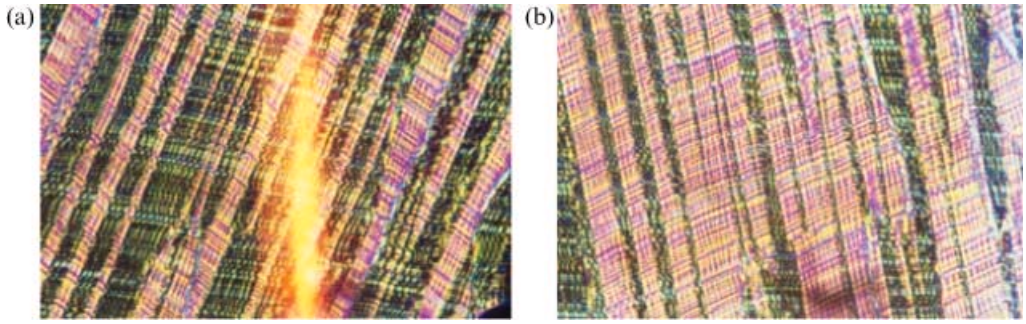

Figure 7. The texture of the SmC_a phase of **4r-8** at 78.2°C in a cell of 5 μm thickness treated for parallel alignment, showing cartridge belt pattern and different birefringence for neighbouring domains. The birefringence of neighbouring domains exchanged when the sample was rotated in the opposite direction by (a) 18° and (b) −14°. The horizontal edge is 0.375 mm.

similar to that of the SmC phase without a field (Figure 9). The same texture change is observed when the field polarity is inverted. The voltage required for this texture change is independent of sample thickness. This texture change resembles that of antiferroelectric to ferroelectric switching of calamitic mesogens, but it takes place only with high voltage. We were unable to carry out the triangular wave study at this high voltage.

For the hockey stick molecules studied here, the results of chemical computation by HyperChem 5.01 MM+ indicated that the dipole moment is pointing out of the molecular plane and tilting away from the aromatic skeleton (*9*). Alignment of these dipole moments to the field direction would tilt the aromatic skeleton away from the substrate normal, which is also the light path. The variation of orientation of aromatic skeleton from the original direction (parallel to substrate surfaces) to this tilted direction is manifested in the observed birefringence changes. This switching behaviour is different from that of calamitic nematogens and is ascribed to the bent conformation. Increasing the field strength would impose a greater restriction on molecular motions and reduce the optical fluctuation. The occurrence of stripe patterns (not shown here) is probably due to an electrohydrodynamic effect (*9*). The parallel orientation of the stripe axis and the original alignment direction is apparently due to the bent conformation, behaviour different from that of Williams domains

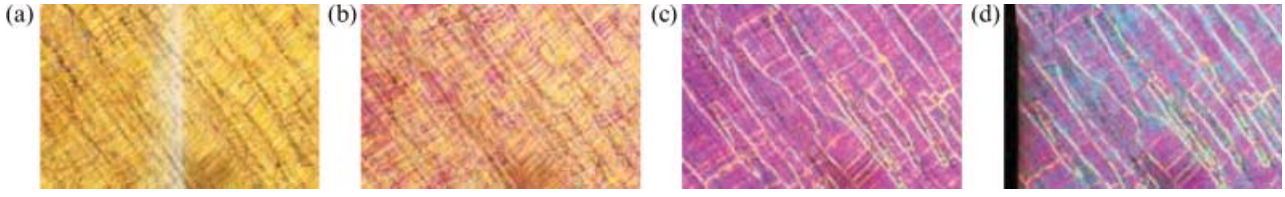

Figure 8. The dc field effects on the SmC_a phase at 113.0°C of the sample shown in Figure 6. The alignment direction is rotated by 45° with respect to the crossed polarisers. The dc field applied was (a) 0, (b) 2, (c) 4 and (d) 6 $V\,\mu m^{-1}$. The horizontal edge is 0.75 mm.

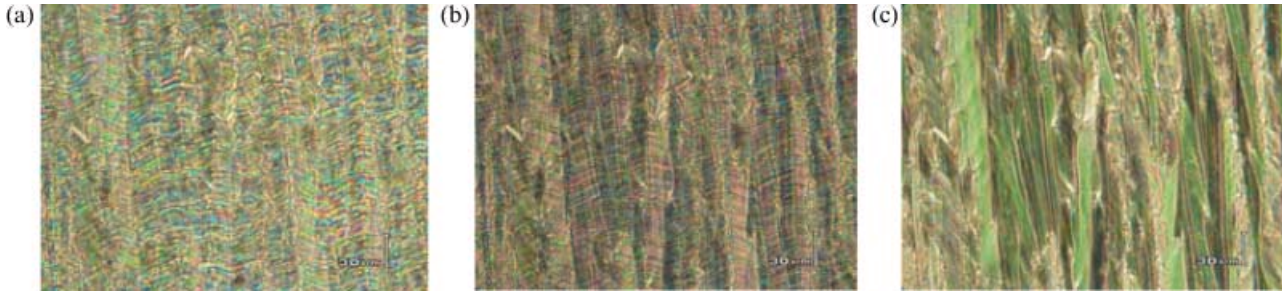

Figure 9. The textures of the SmC_a phase of compound **4r-8** at 108.8°C in an EHC cell of 15 μm thickness with substrate surfaces treated for homogeneous alignment. The applied dc electric voltage was (a) 0, (b) 30 and (c) 300 V. The horizontal edge is 0.375 mm.

observed for calamitic nematogens (*13*). The occurrence of turbulence at slightly higher field strength is due to charged impurities. It occurs only for thicker samples because of the limited penetration distance of surface anchoring force.

The formation of opposite chirality domains and manifested in different birefringence is well known for banana phases, particularly for the B2 and B4 phases (*14*). Furthermore, it has been reported that the different birefringence of neighbouring domains remains unchanged when inverting the polarity of the applied field (*15*). It was suggested therefore that the banana molecules rotated around the long molecular axis, instead of on the cone surface, when the field polarity was switched (*15*). Quite similar behaviours were observed here for the SmC and SmC_a phases of the hockey stick molecules in this study. Both the banana and hockey stick molecules have bent conformation, but the latter has one arm much shorter and with much less polarisability. A medium high value of spontaneous polarisation has been measured for the banana mesogens (*15a*), but the corresponding value for the hockey stick mesogen remains to be verified, *vide infra*.

X-ray study showing clusters in the nematic and simple layer structure in the smectic phases

The X-ray diffraction patterns for non-aligned samples of the N, SmC and SmC_a phases of compound **4r-8** all display a featureless broad hump in the wide-angle region (not shown here) indicating the typical liquid behaviours and no in-layer order for the smectic phases. Figure 10 shows the patterns in the small-angle region for these phases. For the

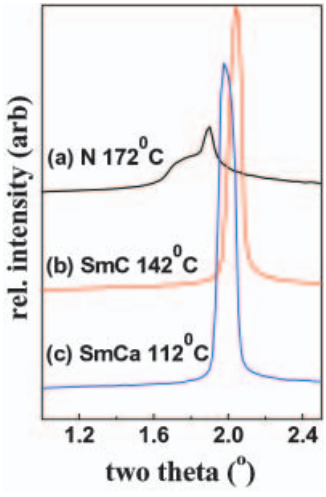

Figure 10. The small-angle X-ray diffraction patterns for a non-oriented sample of compound **4r-8** at (a) 172, (b) 142 and (c) 112°C.

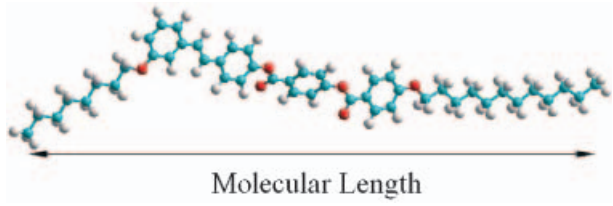

Figure 11. The molecular length of compound **4r-8** is 45.84 Å, as calculated by HyperChem ver.7.5 mm+.

nematic phase, the pattern displays a hump accompanied by a small cusp. The cusp grows at the expense of the hump when the temperature is decreased across the nematic phase. The occurrence of this small cusp is tentatively ascribed to formation of some sort of cybotactic clusters; a cluster of layered structure was originally proposed by de Vries for calamitic nematic phases (*16*). The two-theta values at the hump and the cusp maxima correspond to lengths of 44.90 and 43.41 Å for **4r-8** molecules in the nematic phase. A chemical computation by HyperChem version 7.5 mm+ gives a value of 45.84 Å for the straight distance between the two terminal carbon atoms of the hydrocarbon chains (fully extent all-*trans*-conformation) of **4r-8** (Figure 11). The agreement is reasonable considering that there are many possible rotational conformations allowed for the hydrocarbon chains. A smaller value for the molecules in the cluster is reasonable because of the closer packing restricting the molecular stretching. It is also possible that the molecules are tilted with respect to the layer normal within the cluster.

A single sharp peak is observed for each of the smectic phases (Figure 10). These results clearly indicate that both smectic phases, SmC and SmC_a, are simple layer structures. The layer thickness as a function of temperature is shown in Figure 12, along

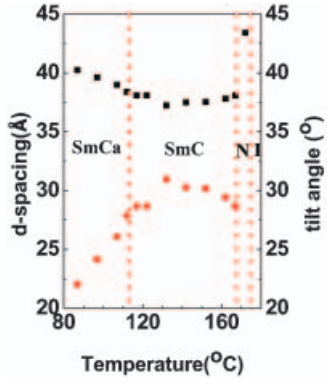

Figure 12. Tilt angle (dots) and d-spacing (squares) as a function of temperature for the SmC and SmC_a phases of compound **4r-8**.

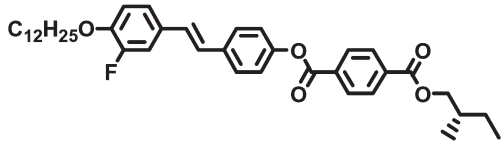

Cr $\xrightarrow[28.47]{70.3}$ SmC* $\xrightarrow[0.08]{155.9}$ SmA $\xrightarrow[1.72]{178.3}$ N* $\xrightarrow[1.64]{180.2}$ I

Scheme 3. Chiral dopant **12MB** and its phase sequence (temperatures in °C, enthalpy changes in kJ mol^{-1} in italics).

with the corresponding tilt angle evaluated with the molecular length (43.41 Å) obtained in the nematic phase. The layer thickness of the SmC phase decreases with temperature and reaches a minimum value of 37.32 Å at about 132°C before increasing again. The layer thickness keeps increasing across the SmC–SmC$_a$ transition, and the growth of layer thickness with respect to temperature is faster in the SmC$_a$ phase. A larger spacing value for the SmC$_a$ phase indicates a smaller tilt angle or an increase of molecular stiffness. This molecular stiffness, or rigidity, is also responsible for transforming the phase structure from synclinic to anticlinic.

The effects of chiral dopant

Calamitic ferroelectric liquid crystals, i.e. chiral SmC phases, can be formed by adding a chiral dopant into a non-chiral SmC host. The purpose here is to see if a similar procedure will induce ferro- and antiferroelectric phases with hockey stick mesogens as the host. The rod-like chiral dopant employed was **12MB**, as depicted in Scheme 3 along its phase sequence and corresponding thermodynamic data. Hockey stick mesogen **3r-4** was used as the host for its similarity in molecular skeleton to the chiral dopant. Table 3 lists the phase sequence and the corresponding thermal properties observed for mixtures containing low mole fractions of **12MB** in **3r-4**. Compared with undoped **3r-4**, it is clear that the mesophases of **3r-4** are retained but with expanded thermal ranges, indicating that the rod-like chiral dopant mixed well with the host molecules although they have different molecular shapes.

The chiral nematic phases observed for the mixtures represent the first example formed by hockey stick mesogen doped with low concentrations of calamitic chiral dopant. Planar textures with oily streaks are observed for the chiral nematics of these mixtures, as shown in Figure 13 a for a mixture containing 10 mol. % of **12MB** in an EHC cell of 2 µm thickness with surfaces treated for homogeneous alignment. The colour of the planar texture remains the same when the sample is rotated, indicating that the helical structure is uniform throughout the sample and the helical axis is perpendicular to the substrates. Upon application of a dc field, a texture of equally spaced finger prints developed (Figure 13 b), indicating that the helical structure is turned by the applied field so that the helical axis is lying in the plane parallel to the substrate. There are domains of various sizes, and the helical axis points to different directions for neighbouring domains. For a yet unknown reason, there are areas of textures with helical axis tilted with respect to the substrates (Figure 13 c). When the field strength is increased, unwinding of the helical structure takes place, resulting in a uniform dark-grey texture (Figure 13 d). This dark-grey texture turns bright when the sample is rotated (Figure 13 e), indicating that the molecules are aligned by the applied field and the molecular axis makes an angle with respect to the

Table 3. Phase transition temperatures (°C) and the corresponding enthalpy changes (kJ mol^{-1}, in italics) of mixtures consisting of the rod-like chiral dopant **12MB** in a hockey stick mesogen **3r-4** (concentrations in mol. %).

3r-4	**12MB**	Cr		SmC$_a$		SmC		SmA		N		I
100	0	·	74.4	·	81.8	·	83.1	·	86.7	–		·
			29.76		*0.26*		*0.16*		*4.09*			
98	2	·	72.0	·	81.5	·	83.2	·	87.6	·	88.1[a]	·
			27.6		*0.22*		*0.15*		*3.67*			
95	5	·	68.3	·	81.2	·	85.3	·	89.5[b]	·	90.0[a]	·
			29.67		*0.15*		*0.15*		*2.76*			
90	10		68.2	·	80.4	·	88.5	·	93.7[b]	·	95.5[a]	·
			27.18		*0.06*		*0.07*		*2.82*			

[a]Overlapped with the neighbouring transition peak. [b]The TGB$_A$ phase is observed in POM, and a broad DSC peak of the N–SmA transition indicates the existence of a TGB$_A$ phase.

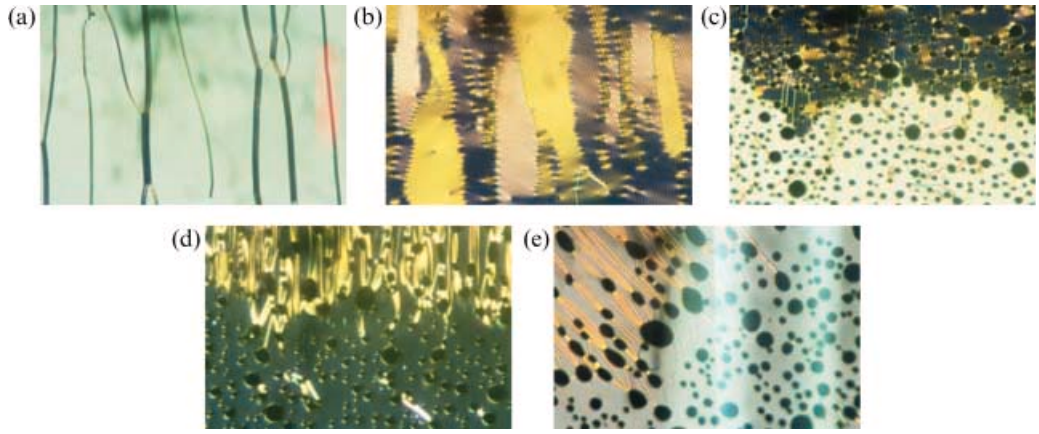

Figure 13. The textures of chiral nematic phase of a mixture consisted of 10 mol. % of calamitic chiral dopant **12MB** in hockey stick mesogen **3r-4**, at 91.0°C. EHC cell, 2 µm, treated for parallel alignment. DC electric field applied was (a) 0, (b) 8, (c) 8, different region, (d) 15 V µm^{-1} and (e) 45° rotattion of (d). The horizontal edge is 0.375 mm.

substrate normal uniformly throughout the sample. Evidently, all of the three molecular axes are aligned simultaneously under this condition, similar to the situation encountered previously for the non-doped nematic phase of hockey stick molecules.

On cooling the chiral nematic, textures of TGB_A phase appeared with vivid colours and existed for a narrow temperature range before focal conic textures of SmA took over for mixtures containing 5 and 10 mol. % of **12MB**. With application of dc fields, these textures changed to long and fan-like textures resembling those of SmA focal conic textures. The SmA phase does not exhibit any electric field activity.

The areas of domains of different types discernible in optical appearance (Figures 14(b) and 14(e)) for the SmC phases of doped mixtures are not in equal fraction, unlike the non-doped SmC having domain areas with equal fraction. The equidistant parallel lines within all domains observed for the non-doped SmC are not observed for the doped sample. Bright and dark textures (or textures of different colours) are observed with application of positive and negative dc electric fields with sample rotated clockwise (Figures 14(a) and 14(c)). The same bright and dark textures can also be observed when the sample is rotated anticlockwise but with the polarity of dc field reversed (Figures 14(d) and 14(f)). Evidently the doped SmC phase displays the characteristic ferroelectric behaviour of a calamitic chiral SmC phase. A maximum contrast ratio between these bright and dark textures can be obtained with certain field strength. This contrast ratio decreases at higher field strength. With much higher field strength the textures remain bright, and the optical appearance remains the same when the field polarity is inverted. This whole process indicates that at a relatively low field strength the ferroelectric behaviour is due to the flipping of molecules on the cone surface, and at much

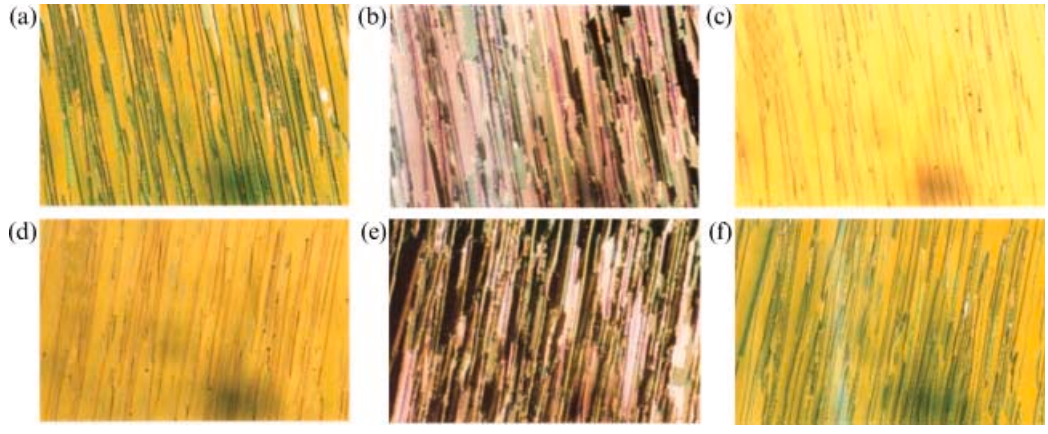

Figure 14. The textures of SmC phase of mixture contained 10 mol. % chiral dopant **12MB** in hockey stick mesogen **3r-4** at 81.6°C. The rotation angle (°) and the applied dc field (V µm^{-1}) were (a) 7 and 10, (b) 7 and 0, (c) 7 and −10, (d) −11 and 10, (e) −11 and 0, and (f) −11 and −10, respectively. The horizontal edge is 0.75 mm.

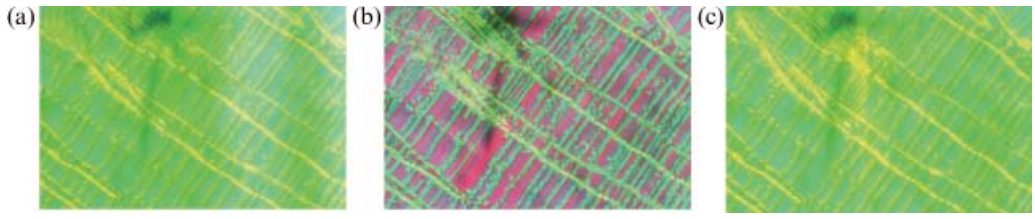

Figure 15. The colour switching of the SmC_a phase of a mixture contained 10 mol. % chiral dopant **12MB** in hockey stick mesogen **3r-4** at 71.1°C. The sample was rotated by 45° and the dc field applied was (a) 20, (b) 0 and (c) $-20\,V\,\mu m^{-1}$. The horizontal edge is 0.75 mm.

higher field strength the molecules are aligned in a fashion more or less like that of the nematic phase aligned by an electric field. For the SmC_a phase of the doped sample, it was also observed that the domains were dominated by one type, (Figure 15(b)). Different colours for the neighbouring domains are observed when the sample is rotated by an angle, and the colours will exchange between the domains when the rotation direction is reversed. Upon application of a dc field, the texture remains unchanged but the difference in colour (or birefringence) diminishes. The same coloured textures are observed when the field polarity is inverted (Figures 15(a) and 15(c)), a behaviour that resembles that of the non-doped SmC_a phase.

The spontaneous polarisation

As one of the main properties to be investigated, the spontaneous polarisation (P_s) of phases formed by these hockey stick molecules was measured with the method of triangular wave of voltage, a common method employed for the calamitic mesogens. However, only a single weak response was recorded for the SmC and SmC_a phases after several attempts with repeating purifications, different thicknesses and various voltages and frequencies. The value of P_s amounts to a few $nC\,cm^{-2}$; this value is ten times the instrumental error obtained by calibration with a known standard. As a further check the mixtures listed in Table 3 were studied with the same method because the chiral compound doped SmC phase exhibited unambiguously the ferroelectric switching behaviour.

A typical result is shown in Figure 16. In the SmC phase, the P_s value increases with decreasing temperature, reaches a maximum and then falls slightly before the temperature approaches the SmC–SmC_a transition. In the SmC_a phase, the P_s value increases steadily with decreasing temperature and drops suddenly when the sample solidifies. All three mixtures displayed a similar P_s temperature dependence pattern in the SmC and SmC_a phases. It is noted that only one current response peak was observed for both the SmC and SmC_a phases after several attempts with triangular wave frequency down to 1Hz. Figure 17 shows the measured P_s values as a function of dopant concentration for these smectic phases. The P_s value is higher in the SmC_a phase than in the SmC phase. The measured P_s value decreases with increasing dopant concentration, an indication that the P_s has opposite sign for the dopant (**12MB**) and the host (**3r-4**). A linear

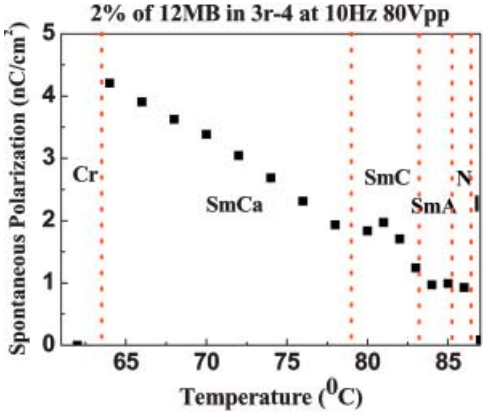

Figure 16. Temperature dependence of spontaneous polarisation of smectic phases of a mixture containing 2 mol. % of chiral dopant **12MB** in hockey stick mesogen **3r-4**.

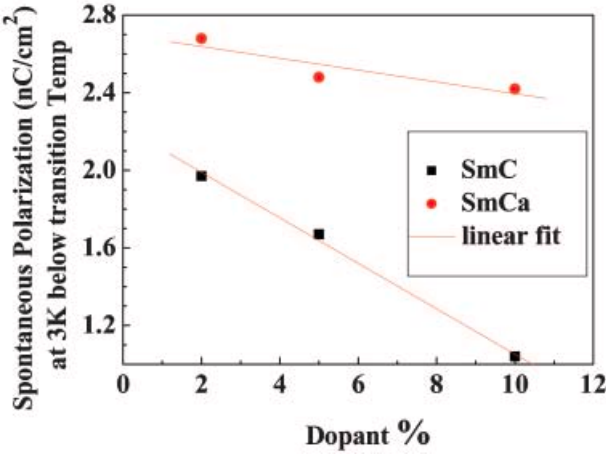

Figure 17. Concentration dependence of spontaneous polarisation of the SmC and SmC_a phases for mixtures containing chiral dopant **12MB** in hockey stick mesogen **3r-4**.

extrapolation of P_s values to zero dopant concentration results in P_s values of 2.2 and 2.7 nC cm^{-2} for the SmC and SmC$_a$ phases, respectively, of compound **3r-4** at temperatures 3 K below the corresponding transition temperatures. These values are comparable to those measured for the non-doped phases.

The molecular organisation

Across the SmC–SmC$_a$ phase transition, the X-ray results show that there is no abrupt change in the layer spacing value, but a drastic texture change is obvious from the optical observation and a transition peak with a very small enthalpy change is obtained from the DSC study. These observations indicate that changes in the phase structure have indeed taken place with nearly no change in the molecular length but accompanied by a rather small energy variation and a sudden change in the polarisation. A possible explanation is the following. The rotational motions of the molecules are partially frozen upon cooling. These partially frozen conformations would render the molecules more rigid or stiffer and therefore a larger separation between the hydrocarbon chains of the neighbouring layers is preferred (the layer spacing increases gradually when temperature is below 132°C). When the SmC–SmC$_a$ transition temperature is reached, the molecule adopts a conformation such that the neighbouring layers switch from synclinic to anticlinic arrangement. Two- and four-brush defects for the SmC and mainly two-brush defects for the SmC$_a$ are observed (*9*). The energy involved is of the value comparable to those observed for the corresponding transition of calamitic mesogens. These conformational variations alter the molecular polarisation and result in an abrupt change of P_s value. With these considerations, a molecular packing for these smectic phases is proposed, as shown in Figure 18. Various layer correlations of smectic phase comprised of bent molecules have been proposed by Brand *et al.* and some of them have been related to the B phases formed by banana mesogens (*17*).

For the SmC phase, viewing on the *y–z* plane (the tilt plane), the molecular directors are tilted to the same direction and the bending directions (the arrow direction) are antiparallel (the bulk polarisation is zero) for the neighbouring layers. All the molecules are rotated to the same direction around an axis perpendicular to the molecular plane. Because the molecular bending directions of neighbouring layers are antiparallel, this arrangement results in an anticlinic configuration when viewed on the *x–z* plane. Below the phase transition temperature, due to the steric hindrance or the repulsion between the hydrocarbon chains an anticlinic arrangement is adopted for the neighbouring layers when viewed on the *y–z* plane for the SmC$_a$ phase. The arrangement remains anticlinic when viewed on the *x–z* plane. These two types of molecular packing would have their own mirror images and constitute the two types of domains observed for these phases.

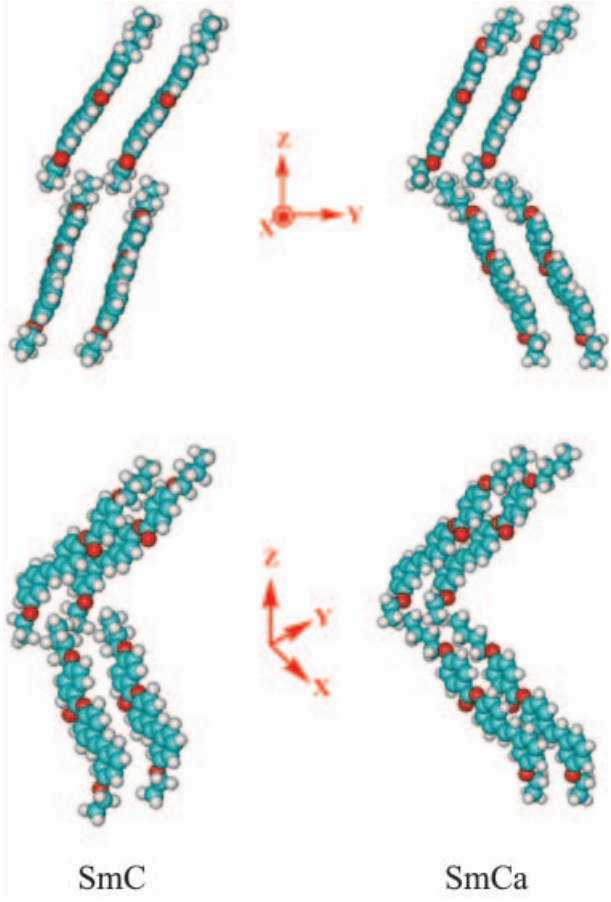

Figure 18. The molecular packing for the SmC and SmC$_a$ phases, left- and right-hand columns, respectively, when viewed on the *y–z* and *x–z* planes, upper and lower row, respectively. The minimum energy conformation of the hockey stick molecule is generated by the HyperChem program, and the same conformational molecules are packed accordingly. The hydrocarbon chain in the SmC$_a$ adopts a different conformation from that in SmC. The number of carbon atoms in the hydrocarbon chains is limited due to the limitation of total number of atoms allowed by the program.

It is interesting to note that the optical study by Huang and co-workers (*6*) shows that chirality is not found in the freestanding films of smectic phases of hockey stick mesogens, and polarisation is observed only for the even-layer films of the anticlinic phase. The optical observations by Hird *et al.* on the mesophases formed by either a racemic or a chiral hockey stick mesogen strongly suggest that a helical structure exists in this phase (*7*). The molecules used in these two studies are all hockey stick in shape, but

the constituting moieties are different. It remains to be studied if the constituents would make such a great difference in this regard. This is highly possible because the degeneracy of conformers of an achiral bent molecule (*9*) would be lifted when the molecule carries a suitable substituent such that one of the conformers exists at a lower energy state. The chirality of banana phases of achiral banana mesogens is a well known example (*4, 14, 15a, 17*). For the observations presented here, sandwich cells with surfaces treated for parallel alignment were used. The anchoring of hockey stick molecule on the surfaces could have set constraints and induced the formation of boundaries between the domains of different smectic layer orientations. The symmetry of the phases having the proposed packing is C_1 so the bulk should be chiral. We were unable to confirm that the highly uniformly spaced parallel lines observed in the domains of the smectic phases are related to the pitch or undulation of smectic layers. These parallel lines were not observed after the chiral dopant was added, for a reason not yet clear. One possibility is that the helical pitch is dilated due to the dopant, a situation that occurs with components having opposite senses of chirality. The ferroelectric switching for the SmC phase after doping is rather clear and resembles that of conventional calamitic ferroelectric switching, a behaviour that might be an indication that the switching of the SmC phase without dopant is not that of the known ferroelectric switching.

4. Conclusion

The results presented here and previously (*9*) indicate clearly that the bent conformation and the polarisability of the constituent moieties are counteracting factors and determine the mesophases to be formed. The phases formed by the achiral hockey stick molecules are the *meso*-phases between the calamitic and banana phases, e.g. the anticlinic smectic phases. Mesophases are stabilised by an increased number of phenyl rings included in the main skeleton, particularly the tilted smectic phases because of the molecular shape. Increasing the *meta*-chain length of hockey stick molecule will lower the isotropisation temperature and stabilise the smectic phases, a behavior similar to that observed for calamitic homologues. However, the anticlinic smectic phase would not be observed if this *meta*-positioned hydrocarbon chain is too long, apparently lacking sufficient polarizability. Anticlinic smectic phases can be stabilised by tuning the *meta*-positioned chain length, the optimal length being six or eight carbon atoms. The thermodynamic properties of mesophases formed by these hockey stick molecules are similar to those of calamitic mesogens. Some optical appearances of these phases when sandwiched between glass substrates without electric field are indiscernible from those of calamitic mesogens, but two-brush defects and two types of domains in the smectic phases are evident. The activities of these phases driven by electric fields, either dc or ac, do not resemble those of calamitic mesogens, and imply that all three molecular axes are simultaneously aligned by the external fields. Corresponding chiral phases are observed when a chiral calamitic dopant is added. The doped SmC phase behaved like the ferroelectric calamitic phase, but similar conversion is not observed for the SmC_a phase. The P_s values measured by the method of triangular wave voltage for the doped and the non-doped smectic phases are comparable. Molecular packing of these smectic phases is proposed on the basis of these observations.

Acknowledgements

This work was supported by the National Science Council contract numbers NSC96-2113-M-032-001 and NSC94-2113-M-032-005. Parts of the electric studies were conducted at the Department of Polymer Engineering of NTUST Taiwan. J.Y. Lee and H. H. Liang are gratefully acknowledged.

References

(1) Meyer R.B.; Liébert L.; Strzelecki L.; Keller P. *J. Phys. Lett., Paris* **1975**, *36*, L69–L71.
(2) (a) Goodby J.W.; Blinc R.; Clark N.A.; Lagerwall S.T.; Osipov M.A.; Pikin S.A.; Sakurai T.; Yoshino K.; Zeks B. *Ferroelectric Liquid Crystals: Principles, Properties and Applications*; Gordon and Breach: Philadelphia, PA, 1991; (b) Lagerwall S.T. *Ferroelectric and Antiferroelectric Liquid Crystals*; Wiley-VCH: Weinheim, 1999.
(3) Niori T.; Sekine T.; Watanabe J.; Furukawa T.; Takezoe H. *J. Mater. Chem.* **1996**, *6*, 1231–1233.
(4) (a) Link D.R.; Natale G.; Shao R.; Maclennan J.E.; Clark N.A.; Körblova E.; Walba D.M. *Science* **1997**, *278*, 1924–1927; (b) Walba D.M.; Körblova E.; Shao R.; Maclennan J.E.; Link D.R.; Glaser M.A.; Clark N.A. *Science* **2000**, *288*, 2181–2184.
(5) (a) Prasad V.; Kang S.W.; Suresh K.A.; Joshi L.; Wang Q.B.; Kumar S. *J. Am. Chem. Soc.* **2005**, *127*, 17224–17227; (b) Acharya B.R.; Primak A.; Kumar S. *Phys. Rev. Lett.* **2004**, *92*, 145506-1; (c) Madsen L.A.; Dingemans T.J.; Nakata M.; Samulski E.T. *Phys. Rev. Lett.* **2004**, *92*, 145505-1; (d) Görtz V.; Goodby J.W. *Chem. Commun.* **2005**, 3262–3264.
(6) (a) Wang S.T.; Wang S.L.; Han X.F.; Liu Z.Q.; Findeisen S.; Weissflog W.; Huang C.C. *Liq. Cryst.* **2005**, *32*, 609–617; (b) Han X.F.; Wang S.T.; Cady A.; Liu Z.Q.; Findeisen S.; Weissflog W.; Huang C.C. *Phys. Rev. E* **2003**, *68*, 060701; (c) Stannarius R.; Li J.J.; Weissflog W. *Phys. Rev. Lett.* **2003**, *90*, 025502;

(d) Das B.; Grande S.; Weissflog W.; Eremin A.; Schröder M.W.; Pelzl G.; Diele S.; Kresse H. *Liq. Cryst.* **2003**, *30*, 529–539.
(7) Hird M.; Goodby J.W.; Gough N.; Toyne K.J. *J. Mater. Chem.* **2001**, *11*, 2732–2742.
(8) Fergusson K.M.; Hird M. *Adv. Mater.* **2007**, *19*, 211–214.
(9) Yu F.C.; Yu L.J. *Chem. Mater.* **2006**, *18*, 5410–5420.
(10) (a) Heck R.F. *J. Am. Chem. Soc.* **1968**, *90*, 5518–5521; (b) Heck R.F. *Accts Chem. Res.* **1979**, *12*, 146–151; (c) Heck R.F. *Org. React.* **1982**, *27*, 345–390.
(11) Kocienski P.J. *Protecting Groups*; Georg Thieme Verlag: Stuttgart, 1994. p. 120.
(12) (a) Weissflog W.; Nadasi H.; Dunemann U.; Pelzl G.; Diele S.; Eremin A.; Kresse H. *J. Mater. Chem.* **2001**, *11*, 2748–2758; (b) Dunemann U.; Schröder M.W.; Amaranatha Reddy R.; Pelzl G.; Diele S.; Weissflog W. *J. Mater. Chem.* **2005**, *15*, 4051–4061 and references therein; (c) Shreenivasa Murthy H.N.; Sadashiva B.K. *Liq. Cryst.* **2004**, *31*, 567–578.
(13) (a) de Gennes P.G.; Prost J. *The Physics of Liquid Crystals*; Oxford University Press: New York, 1993; (b) Demus D.; Goodby J.W.; Gray G.W.; Spiess H.W.; Vill V. *Handbook of Liquid Crystals*; Wiley-VCH: Weinheim, 1998.
(14) (a) Choi S.W.; Kang S.; Takanishi Y.; Ishikawa K.; Watanabe J.; Takezoe H. *Angew. Chem. Int. Ed.* **2006**, *45*, 6503–6506; (b) Niwano H.; Nakat M.; Thisayukta J.; Link D.R.; Takezoe H.; Watanabe J. *J. Phys. Chem. B* **2004**, *108*, 14889–14896; (c) Thisayukta J.; Niwano H.; Takezoe H.; Watanabe J. *J. Am. Chem. Soc.* **2002**, *124*, 3354–3358.
(15) (a) Weissflog W.; Dunemann U.; Schroder M.W.; Diele S.; Pelzl G.; Kresse H.; Grande S. *J. Mater. Chem.* **2005**, *15*, 939–946; (b) Amaranatha Reddy R.; Raghunathan V.A.; Sadashiva B.K. *Chem. Mater.* **2005**, *17*, 274–283.
(16) de Vries A. *Mol. Cryst. liq. Cryst.* **1970**, *10*, 219–236.
(17) (a) Brand H.R.; Cladis P.E.; Pleiner H. *Eur. Phys. J. B* **1998**, *6*, 347–353; (b) Brand H.R.; Cladis P.E.; Pleiner H. *Int. J. Engng Sci.* **2000**, *38*, 1099–1112.